DIFFERENT TYPES OF LATTICES AND ITS SIGNIFICANCE

Parihar Sarika Indersing, Research Scholar (Physics), SunRise University, Alwar (Rajasthan).
Dr. Priyanaka Garg, , Research Supervisor (Physics), SunRise University, Alwar (Rajasthan).

INTRODUCTION

Colloidal nanoparticles have the ability to self-assemble into enormous two-dimensional films or three-dimensional mesoscopic arrays (Figure), which are also referred to as nanoparticle supercrystals, nanoparticle supra-crystals, nanoparticle superlattices, or nanoparticle assemblies. Nanoparticles, much like atoms in crystals, display long-range translational order when they are assembled into nanoparticle assemblies. When nanoparticle assemblies have orientational order, we refer to them as mesocrystals. This means that the nanoparticle building blocks demonstrate coherent alignment of their crystal axes. 48 Nanoparticle assemblies are appealing for the construction of complicated functional devices, and the assembly process in and of itself is fascinating for basic study on crystallization49–51. 52–57 The evaporation of a colloidal dispersion under controlled circumstances is frequently what sets off the process of nanoparticle building. 49,58,59 Destabilization of the colloidal dispersion (such as depletion and non-solvent destabilization),60,61 induced assembly by external magnetic62 and electric fields63 or light64,65 and DNA mediated-assembly are some of the additional techniques that may be exploited. 66,67 Nanoparticle assemblies (such as 2D films and 3D mesoscopic arrays of singleand multiple-component nanoparticle assemblies) with a large structural diversity have been developed as a result of significant research efforts over the past decade. These efforts have led to the development of nanoparticle assemblies.

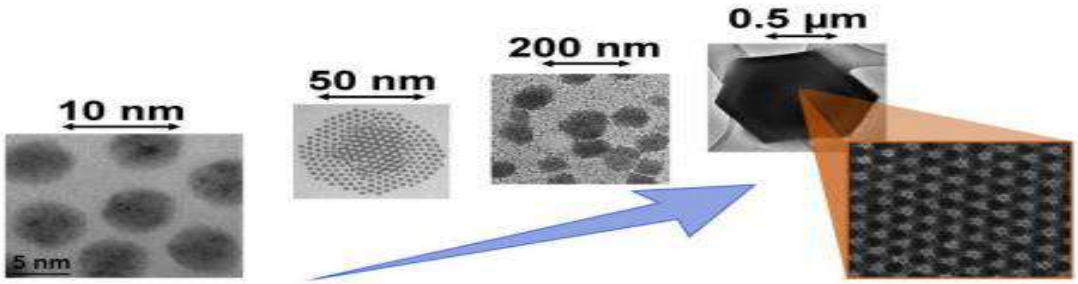

Figure: Self-assembly of spherical nanoparticle into ordered mesoscopic nanoparticle assemblies?

A POWERFUL TOOL TO INVESTIGATE LATTICE

The use of transmission electron microscopy (TEM) has unquestionably evolved into a powerful and flexible instrument for the investigation of the structures of materials, in particular nanomaterials. It is to one's benefit to employ electrons as a source due to the fact that they interact intensely with matter. 73 Because of this, electrons may be used to investigate minuscule individual crystals or atomic clusters with sizes ranging from a few angstroms to hundreds of nanometers. Electrons interacting with matter produce a variety of signals (such as elastic/inelastic scattered electrons, photons, and so on) that can be used to obtain information on the structure, chemical nature, and physical properties of a material. These signals include elastic/inelastic scattered electrons, photons, and so on (e.g. optical, magnetic and electrical properties). Traditional high-resolution imaging, in conjunction with electron diffraction, has been put to considerable use for the structural investigation of a broad variety of materials, including phase identification, structure determination, and the localization of interfacial defects. 74–76 Researchers are now able to examine material structures at an atomic resolution thanks to recent technical breakthroughs in TEM optics (such as monochromators, aberration correctors, and detectors), as well as revolutionary TEM-based methodologies that include the application of robust algorithms. Reliability in establishing the three-dimensional structural model of nanocrystals has recently been established by methods based on three-dimensional TEM (in both real and reciprocal space). 77,80,81 For instance, the three-dimensional core structure of an edge dislocation may be recognised in multiply-twinned Pt nanoparticles. [Citation needed] 82 In addition, electron diffraction tomography has shown to be effective when applied to the task of determining the structure of complicated sub-micron crystals. 83,84 The development of tools for image analysis has opened up new opportunities

for obtaining important information on the atomic arrangement and local structural inhomogeneities in nanoparticles. These new possibilities have been made possible as a result of the development of image analysis technologies (e.g. lattice strain). For instance, atomic resolution electron tomography was used to successfully show three-dimensional assessment of the lattice strain in gold nanoparticles. 85 Chemical mapping at atomic resolution was accomplished using scanning transmission electron microscopy (STEM) imaging paired with either energy-dispersive X-ray spectroscopy (EDS) or electron energy-loss spectroscopy (EELS). 86– 92 Transmission electron microscopes may also be used in the investigation of other physical characteristics, such as the magnetism of nanomaterials by the use of electron holography93 or electron magnetic circular dichroism (EMCD).

ANALYSES OF THE DIFFERENT LATTICE PARAMETERS

The estimated values of d were discovered to change depending on the length of time an experiment lasted and the temperature at which it was conducted. When the temperature rises, the particles get larger in size. The 'D' values range from 26 nm to 43 nm to 26 nm in ZNS #7 to #10, all of which employ ammonia as a mineralizer; these values are, respectively, 26 nm, 26 nm, and 43 nm. These values are discovered to be dependent on the circumstances of the experiment; for example, the 'D' value is found to be larger when either the temperature or the time length of the experiment is found to be higher. Both ZNS #9 and #10 are identical in their respective comparable morphologies. Nevertheless, when NaOH was employed as the mineralizer, it was discovered that these values did not have any impact on the parameters of the experiment. It's possible that the various morphologies of the nanostructures are to blame for this kind of independence. Pictures show electron micrographs of all of the consequent morphologies that were presented by 10 distinct ZNS. The c/a ratio that is considered typical in the JCPDS card is 1.6023. The change in c/a of the ZNS that was produced by subjecting it to the hydrothermal treatment for varying amounts of time while maintaining all of the other hydrothermal conditions is seen in Figure. The value of c/a falls between the hours of four and sixteen, and then it begins to rise again between the hours of sixteen and eighteen. The c/a number shown by the horizontal straight line is the standard value. It is interesting to notice that the ZNS generated in 16 and 18 hours, which had the closest value to the norm, were well-defined nanorods, but the ZNS produced in 4 and 16 hours were nanoflakes and nanopetals, respectively. The ZNS that was generated from the mother solutions with the lowest pH (9.5) and the highest pH (13.5) were found to demonstrate a nearness to the standard c/a, however the ZNS that was formed from the mother solutions with pH 10.5 and 12 showed a minor departure, as seen in figure.

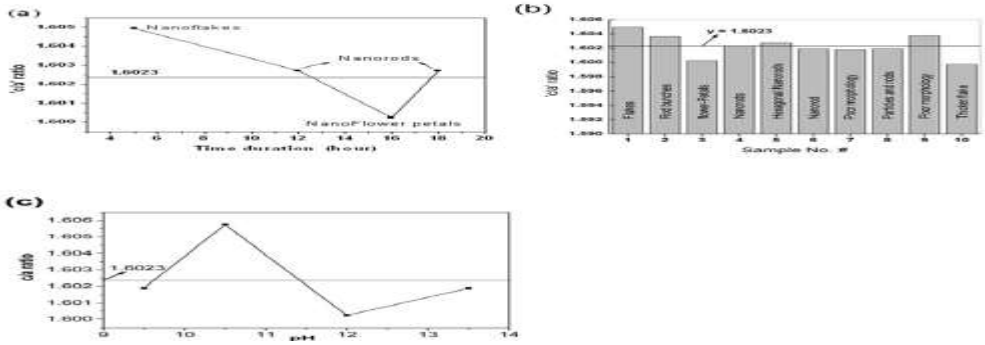

Figure: A plot displaying the c/a ratio of the various structures generated throughout the various time durations of the experiment; (b) a comparison of the various c/a values of all of the formed structures; and (c) a change of c/a with time duration of the experiment.

IMPACT OF LATTICES

Experimental Details

In this experiment, two distinct strengths of NaOH, 1.5M and 2.5M, are reacted with five distinct concentrations of zinc acetate dihydrate, ranging from 0.02M to 0.1M and increasing by 0.02M from the preceding concentration. This allowed for the formation of 10 distinct permutations of cationic and anionic strengths. Zinc acetate dihydrate solutions of concentrations 0.02 M, 0.04 M, 0.06 M, 0.08 M, and 0.1 M are prepared in separate containers, each containing two quantities of the solution. One of them at each of the five different

concentrations is reacted with 15 ml of a solution that has a concentration of 1.5M NaOH. In another set, a solution of 2.5 M NaOH was added, with 15 ml of it placed in each of the containers. The experiment that was conducted with 1.5 M of NaOH and 0.02M of Zn2+ was given the code Z11 so that it would be simple to identify. The number one on the left represents the concentration of the mineralizer, and the number one on the right represents the cationic strength (#1 minus 0.02M of Zn2+). Following this pattern, "Z12" refers to 1.5 M of NaOH and 0.04 M of Zn2+, and so on. "Z21" is the designation given to the mixture that consists of 2.5M of NaOH and 0.02M of Zn2+, and so on. In the experiment for the concentration of 0.02 M Zn salt, 1.5 M of NaOH solution, the mixture was agitated thoroughly until a homogenous solution is achieved. The clear details of the combinations that were tested with along with their morphologies derived from SEM pictures are provided in Table. The mother liquor was well mixed before being transferred to an autoclave made of Teflon-lined stainless steel. When the autoclave had been filled with solution up to a filling ratio of 80% and had been securely shut, the mixture that was contained inside it was subjected to hydrothermal treatment for a period of four hours at a temperature of 180 degrees Celsius. In a similar manner, each of the other possible combinations is mixed together before being poured into the autoclave.

In every single one of the tests, the circumstances of the response were kept exactly the same. When the reaction had been completed, the autoclave was let to cool down normally to the surrounding temperature. After that, the particles that had been separated by many rounds of centrifugation were given multiple washes in demineralized water and ethanol in order to get rid of any ionic impurities that could have been present. In the instances with a higher concentration, the Zn salt concentration is 0.8, which means that the yield will definitely be greater; nevertheless, these cases need to be washed a few more times than the examples with a lower concentration. After that, the white powders were removed from their solvents by being baked in a hot air oven at a temperature of 120 degrees Celsius for a few hours. After that, the dry white powder was saved and put to use for more research and examination.

XRD Analysis:

Calculations have been done to determine the following parameters based on the Full Width at Half Maximum of x-ray reflection lines: I the u parameter; (ii) the cell volume; and (iii) the lattice distortion. As compared to the architectures of zinc blende and rock salt, the wurtzite structure of ZnO, which is characterised by a hexagonally close-packed arrangement, is much more stable. In ZnO, the atoms of zinc and oxygen are connected to one another in a tetrahedral fashion. The parameters of the ZnO lattice are set up in such a way that they maintain the ratio c/a = 83 = 1.633. This structure occurs naturally with two interpenetrating sublattices, and the two atoms that make up the structure are displaced by each other by a distance equal to u = 3/8 = 0.375 angstroms. This 'u' value is equivalent to the length of the bond that is perpendicular to the c-axis, measured in units of the 'c' value's 'a2' dimension. The equation for the relation is u4=c2=3, and it may be written down as such. So, it should come as no surprise that the structure of zinc oxide does not perfectly match that of the ideal wurtzite. This is spontaneously modified by changing the value of 'c/a' and 'u' that is included inside it. The value of 'u' for each of the nanostructures was determined using the x-ray reflection spectrum, and the results are shown in Table below.

Table The line broadening of x-ray reflection lines provided the basis for deriving the lattice parameter values of the various nanocrystalline forms of ZnO..

Sample ID	a Å	c Å	'u' parameter	Cell Volume Å ^{3}	Lattice Distortion (Vo-V/Vo)
ZnO # 1	3.291	5.227	0.382139	49.02766	0.03016
ZnO # 2	3.292	5.227	0.382219	49.05746	0.030786
ZnO # 3	3.307	5.22	0.383785	49.43924	0.038808
ZnO # 4	3.285	5.234	0.381305	48.91448	0.027781
ZnO # 5	3.289	5.227	0.381978	48.96809	0.028908
ZnO # 6	3.289	5.212	0.382739	48.82757	0.025955
ZnO # 7	3.287	5.249	0.380715	49.11441	0.031982
ZnO # 8	3.300	5.241	0.382153	49.42822	0.038576
STANDARD	3.249	5.206	0.379828	47.59228	----

The 'u' parameter, cell volume, and lattice distortion were subsequently determined using the results of the earlier calculations Since the actual values of the wurtzite lattice parameter values never quite match up with those of the ideal or standard wurtzite structure, it is only logical that the variations in the wurtzite lattice parameter values would result in a change to the volume of the unit cell. The distinction is referred to as lattice distortion in this context, and the value of the difference may be determined using the following relation.

$$\text{Lattice distortion} = \frac{Vo - V}{Vo}$$

Here, 'Vo' – refers for the standard volume of the cell and is equal to 47.59228 Å \s as per the lattice specifications in the JCPDS standard card. The letter 'V' denotes the cell volume that was calculated based on the x-ray diffraction data of the nanostructure that was of interest. The lattice distortion values i.e., the divergence of cell volumes of the hydrothermally generated nanostructures from the standard cell volume is listed in Table.

CONCLUSION

The time length and temperature of the hydrothermal treatment have been discovered to have substantial impact on the creation of well defined distinctive hexagonal shape of ZnO. The difference in the population of growth units and nuclei are discovered to determine the shape of the nanostructure. It was observed that the predicted particle size was not directly reliant simply on the experimental parameters. This was because the particles generated had diverse morphologies. As compared to non-geometrical morphologies such as nanoflakes-like and nanopetals-like structures, well-defined typical hexagonal ZnO nanorods do demonstrate excellent standard lattice parameter values. Time length of 16-18 hours and the mother solution with pH 9.5, 13.5 do result with the lattice parameters closer to the standard value. (SECTION A) Hydrothermal experiments create zinc oxide nanostructures with a wide variety of morphologies and aspect ratios by adjusting the ionic strengths of the solution. These nanostructures are described in more detail below. The function that the ionic strength plays in changing the interfacial energy of the system and, as a result, the particle size is shown in a straightforward and convincing manner. We examine a variety of settings, or ambiences, in which homogeneous and heterogeneous nucleations may potentially be created. On the basis of the energy required for the development of nuclei, one may explain the formation of agglomeration of laterally formed nuclei onto previously grown nanocrystals, which is one of the probable causes for the formation of agglomeration. In conclusion, a straightforward technique for modifying the essential physical entities during the hydrothermal formation of ZnO nanostructures has been investigated and thoroughly reported on.

The Findings and Our Discussion of Them

The X-ray diffraction pattern, which can be seen in Figure, has been determined to have the same pattern as that of pure hexagonal ZnO, which can be found on JCPDS standard card no. 36-1451. There was no discernible difference in the X-ray diffractograms between any of the different surfactant concentrations. The unusual nanorod bunches like structures that were generated by utilising different concentrations of CTAB are shown in the scanning electron micrographs (Figure.). Debye-formula Scherrer's was used to the data obtained from the X-ray study, which included the interplanar spacing and the Full Width Half Maximum (FWHM), to calculate the average particle size.

$$d = \frac{0.9\lambda}{B\cos\theta_B}$$

With the exception of the 6:1 ratio, the computed particle sizes were found to be in the range of 22 to 29 nm for all of the other examples, demonstrating that the addition of surfactant improves the average particle size. The number of dislocation lines that are present in a given region is what is referred to as the dislocation density.

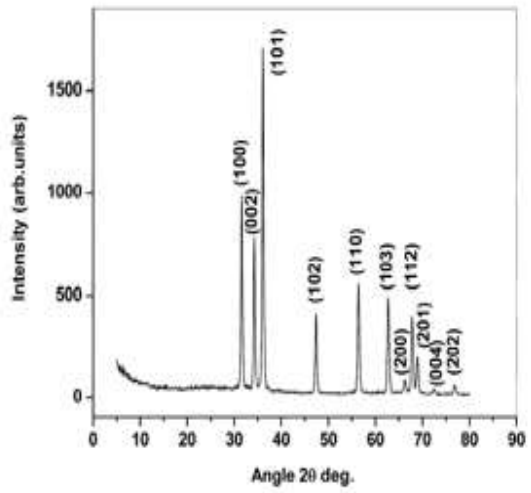

Figure: X-ray diffraction pattern of Zn: CTAB with all its characteristic peaks.

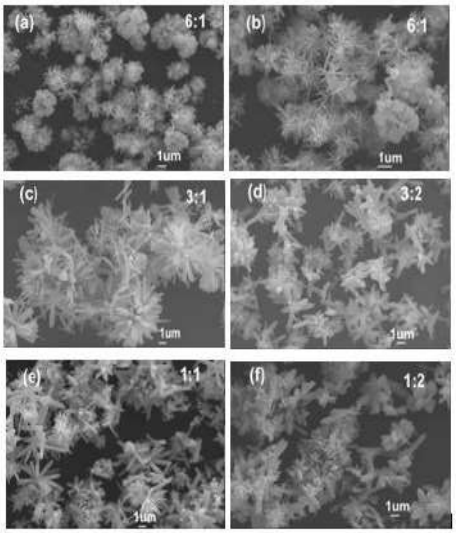

Figure: pictures taken with a scanning electron microscope showing varying concentrations of Zn: CTAB.

On each picture is written the Zn precursor ratio that corresponds to it, as well as the surfactant ratio.

The combination with the lowest concentration of CTAB was found to have the highest dislocation density, which was measured at 25 x 106 lines per unit length/volume. In comparison, the combination with the equal ratio had a value of 18 x 106 lines per metre, and all of the other combinations showed values that were close to or slightly above 13 x 106. As a result of this, it has been shown beyond a reasonable doubt that the decrease in dislocation density may be attributed to the rise in concentration. With the production of micelles in the solution, it is hypothesised that all of the active sites would have the same rate of development. When there is a higher micelle concentration, this homogeneity may be seen more clearly. If there is a lower concentration of CTAB, then there will be a smaller number of active sites, but the total number of growth units will be greater. As a consequence of this, the negatively charged particles engage in a competition with one another in order to attach themselves to the active sites of the cationic surfactant. As a direct consequence of this, a quick growth transpires, which results in an abnormally high number of dislocations. As a result, the dislocation density may be brought back under control by raising the concentration of the surfactant. The lattice parameters for a system with a hexagonal structure may be obtained using

$$\text{Dislocation density } \rho = \frac{\sqrt{12\langle e^2 \rangle}}{dp} \qquad (3.2)$$

p → particle size (obtained from Debye Scherer's formula)

$\langle e^2 \rangle^{1/2}$ → RMS strain

d → interplanar spacing

After replacing the 'd' value of the (hkl) peaks (100) and (002), the values of the lattice parameter 'a' and 'c' are subsequently determined, as is the ratio (c/a). According to the JCPDS, the value that is determined for 'c/a' is 1.6023. This number pertains to the standard lattice parameters. According to our findings, the 'c/a' values that were computed fall within the range of 1.600 for all of the three intermediate combination ratios (3:1, 3:2, 1:1), and they fall between 1.598 and 1.599 for the lowest and greatest CTAB concentrations correspondingly. It has been shown that, at a concentration of CTAB that is considered to be moderate, the lattice parameters do not exhibit a significant amount of variance. The CTAB concentrations with the least and

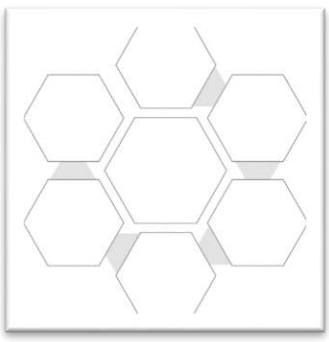

most deviation in their lattice parameters are those with the lowest and greatest respective concentrations. It is important to note that the fluctuation in the lattice parameter is consistent with the predicted average crystallite size. Table has a tabular representation of all the findings of the computed parameters, which may be used for comparison.

X-ray diffraction: a structural analysis tool

According to the findings of the X-ray powder diffraction examination, all three of the amines that were selected resulted in the production of the same material, which was wurtzite structured ZnO. Each of the typical diffraction patterns shown in Figure has all of the peaks that are distinctive of the pattern. It was discovered via the use of line broadening in the calculations that the addition of ethanolamines did not change the characteristics of the lattice. These findings were uncovered. The produced nanoparticles had crystallite diameters that ranged from 20 to 50 nanometers on average, according to the measurements taken. As compared to the other nanostructures that were generated using the same quantity of other precursors, the addition of NaOH resulted in a larger crystallite size than was seen in the other nanostructures. Without NaOH.

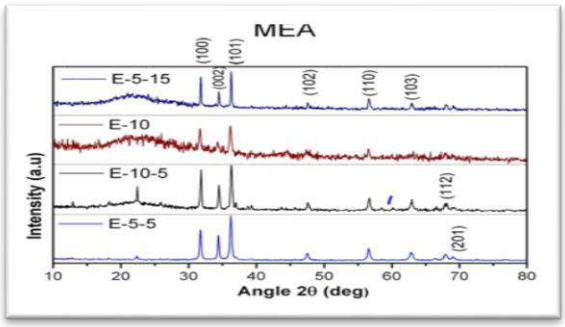

Figure: X-ray diffractograms of ZnO nanostructures that were produced using monoethanolamine and sodium hydroxide respectively

Even though it was discovered that some of the unit cell volumes made employing ethanolamines have been found to slightly deviate from the standard value, it was discovered that the majority of the nanostructures formed have a nearness to the standard value. While looking at the XRD patterns of ZnO nanoparticles formed from primary, secondary, and tertiary ethanolamines, it was discovered that development along certain directions is preferentially favoured or selectively prevented. This was discovered by analysing the patterns. Images taken with a scanning electron microscope have shown us that the three different ethanolamines produce forms that are distinct from one another. In addition to this, the XRD patterns provide some insight into the relative growth rates of the many typical growth faces of zinc oxide. Yet, when it comes to monoethanolamine (MEA), the strength along the (002) orientation is reduced when compared to the other three prominent orientations.

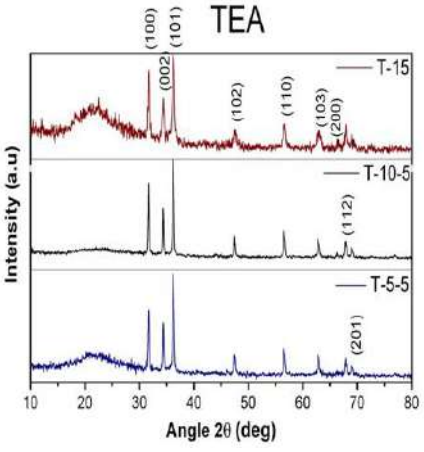

Figure: XRD patterns of ZnO nanostructures prepared using Triethanolamine and NaOH.

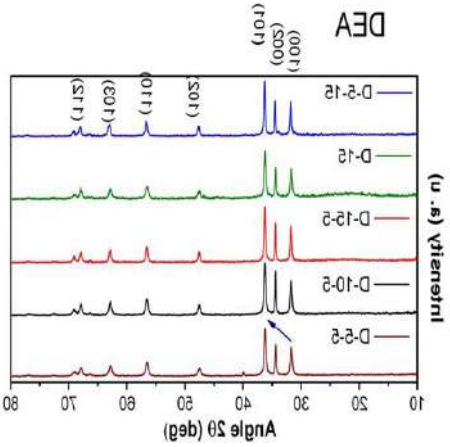

Figure:XRD- patterns of ZnO nanostructures produced using Diethanolamine and NaOH.

The strength of the peaks (100), (002), and (101) for diethanolamine can be seen to increase from lowest to highest. In contrast, the peak intensities of (100) and (002) are closer together for triethanolamine, although the peak (101) has the greatest intensity. The peak (002) is an example of the axial growth that occurs in hexagonal shape. The decrease in the intensity of (002) is a sign that the rods are becoming shorter.

REFERENCES

1. M.C. Kao, H.Z. Chen, S.L. Young, Thin solid films 519 (2011) 3268–3271. M.A.A. Aviles, Y. Wu, J. Am. Chem. Soc. 131(2009) 3216–3224.
2. B. Tan, E. Toman, Y. Li, Y. Wu, J. Am. Chem. Soc.129 (2007) 4162–4163.
3. T.L. Villarreal, G. Boschloo, A. Hagfeldt, J. Phys.Chem. C 111 (2007) 5549–5556.
4. Anaraki Firooz, A. Reza Mahjoub, A. Ali Khodadadi, M. Mova hedi, Chem. Eng. J. 165 (2010) 735–739.
5. M. J. Kim, S. H. Park, Y. D. Huh, Bull. Korean Chem. 32 (2011) 1757–1760.
6. B. Gao, H. Fan, X. Zhang, L.Song, Mater. Sci. Eng. B 177 (2012) 1126–1132.
7. P. K. Chen, G. J. Lee, S. Anandan, Jerry J. Wu, Mater. Sci. Eng. B 177 (2012) 190–196.
8. Wyckoff, R.W.G. Crystal Structures, 2nd ed; Wiley: New York, 1964 p. 238 150 Chapter 7.
9. Z. Y. Fan, H. razavi, J. W. Do, A. Moriwaki, O. Ergen, Y.L. Chueh, P. W. Leu, J. C. Ho, T. Takahashi, L. A. Reichertz, S. Neale, K. Yu, M. Wu, J. W. Ager, A. Javey, Nature Materials 8 (2009) 648–653.
10. Z. Y. Fan, R. Kapadia, P.W. Leu, X. b. Zhang, Y.L. Chueh, K. Takei, K. Yu, A. Jamshidi,
11. A. Rathore, D. J. Ruebusch, M. Wu, A. Javey, Nano Letters 10 (2010) 3823–3827.
12. Y.L. Chueh, Z. Y. Fan, K. Takei, H. Ko, R. Kapadia, A. Rathore, N. Miller, K. Yu, M. Wu,
13. E. E. Haller, A. Javey, Nano Letters 10 (2010) 520–523.
14. Guozhong Cao, Nanostructures and Nanomaterials: Synthesis, Properties and Applications (2004), Imperial College Press (World Scientific Publishing Co. Pte. Ltd.) ISBN 1-86094- 415-9.